Contributions of Stratospheric Water Vapor to Decadal Changes in the Rate of Global Warming

Susan Solomon,[1] Karen H. Rosenlof,[1] Robert W. Portmann,[1] John S. Daniel,[1] Sean M. Davis,[1,2] Todd J. Sanford,[1,2] Gian-Kasper Plattner[3]

Stratospheric water vapor concentrations decreased by about 10% after the year 2000. Here we show that this acted to slow the rate of increase in global surface temperature over 2000–2009 by about 25% compared to that which would have occurred due only to carbon dioxide and other greenhouse gases. More limited data suggest that stratospheric water vapor probably increased between 1980 and 2000, which would have enhanced the decadal rate of surface warming during the 1990s by about 30% as compared to estimates neglecting this change. These findings show that stratospheric water vapor is an important driver of decadal global surface climate change.

O ver the past century, global average surface temperatures have warmed by about 0.75°C. Much of the warming occurred in the past half-century, over which the average decadal rate of change was about 0.13°C, largely due to anthropogenic increases in well-mixed greenhouse gases (1). However, the trend in global surface temperatures has been nearly flat since the late 1990s despite continuing increases in the forcing due to the sum of the well-mixed greenhouse gases (CO_2, CH_4, halocarbons, and N_2O), raising questions regarding the understanding of forced climate change, its drivers, the parameters that define natural internal variability (2), and how fully these terms are represented in climate models. Here we use a combination of data and models to show that stratospheric water vapor very likely made substantial contributions to the flattening of the global warming trend since about 2000. Although earlier data are less complete, the observations also suggest that stratospheric water contributed to enhancing the warming observed during 1980–2000 [as emphasized in previous studies (3–5)].

Water vapor is a highly variable gas. Tropospheric water vapor increases in close association with warming (6), and this represents a major climate feedback that is well simulated in global climate models (7). In sharp contrast, current global models are limited in their representations of key processes that control the distribution and variability of water within the stratosphere, such as the deep convection that affects the temperatures at which air enters the stratosphere and the resulting drying (8). Current global climate models simulate lower-stratospheric temperature trends

poorly (9), and even up-to-date stratospheric chemistry-climate models do not consistently reproduce tropical tropopause minimum temperatures (10) or recently observed changes in stratospheric water vapor (11). Because of these limitations in prognostic climate model simulations, here we impose observed stratospheric water vapor changes diagnostically as a forcing for the purpose of evaluation and comparison to other climate change agents. However, in the real world, the contributions of changes in stratospheric water vapor to global climate change may be a source of unforced decadal variability, or they may be a feedback coupled to climate change, as discussed further below.

Increases in stratospheric water vapor act to cool the stratosphere but to warm the troposphere, whereas the reverse is true for stratospheric water vapor decreases. Previous studies have suggested that stratospheric water vapor changes might contribute significantly to climate change (3–5), but there has been debate about the magnitude of the radiative effects (12) as well as whether systematic changes in water vapor could be documented, because of calibration issues (13) and limited spatial coverage before the mid-1990s. Beginning in 1980, information on trends in stratospheric water was based largely on balloon observations from a single site in Boulder, Colorado (14), but high-quality global satellite observations from multiple platforms began in the 1990s. A substantial and unexpected decrease in stratospheric water vapor was documented after the year 2000 (15), and lower levels have persisted up to the present (mid-2009, see Fig. 1). Here we use a range of recent observations of stratospheric water vapor coupled with detailed radiative transfer and modeling information to describe the global changes in this important species and to estimate their expected impacts on climate trends.

Recent global stratospheric water vapor changes. Data used to assess global changes in stratospheric water vapor are from the HALogen

Occultation Experiment (HALOE) that flew on the Upper Atmosphere Research Satellite (UARS) from late 1991 through November 2005, with coverage extending from the tropopause to the stratopause over 65°S to 65°N (16). Figure 1A shows the time series of mid-latitude water vapor in the lower stratosphere based on HALOE and balloon sonde measurements (17), along with two additional (and independent) sets of satellite data from the Stratospheric Aerosol and Gas Experiment II (SAGE II) (18) and from the Microwave Limb Sounder (MLS) (19) instruments. Taken together, these data provide strong evidence for a sharp and persistent drop of about 0.4 parts per million by volume (ppmv) after the year 2000. Observations of lower-stratospheric tropical ozone changes also reveal a sharp change after 2000 (15). Before this decrease, the balloon data suggest a gradual mid-latitude increase in lower-stratospheric water vapor of more than 1 ppmv from about 1980 to 2000. The HALOE data as well as other Northern Hemisphere mid-latitude data sets also support increases in lower-stratospheric water vapor during the 1990s of about 0.5 ppmv (15, 20).

Using HALOE data, the annual average water vapor difference before and after the persistent drop at the end of 2000 is contoured in Fig. 1B. Averages were constructed on a seasonal basis for two comparison periods, from 1996–2000 and for 2001.5–2005.5. Only measurements above the tropopause were used; i.e., water vapor changes in the troposphere were not included in the analysis. Figure 1B shows that substantial water vapor decreases after 2000 extend throughout the bulk of the stratosphere, with the largest magnitudes in the lowermost tropical and subtropical stratosphere.

The water vapor content of the stratosphere is controlled by transport through the tropopause region (21) and the oxidation of methane within the stratosphere. Transport into the stratosphere occurs mainly as air rises in the tropics and is largely a function of the coldest temperature encountered, or the cold point (8, 22–24). The drop in stratospheric water vapor observed after 2001 has been correlated (25) with sea surface temperature (SST) increases in the vicinity of the tropical warm pool (Fig. 1C), which are related to El Niño–Southern Oscillation; the maximum correlation between stratospheric entry values of water vapor and cold point temperatures was found just to the west of the warmest SSTs (10°N to 10°S; 171° to 200°W). Figure 1C shows that although the water vapor changes appear to be positively correlated with SSTs after about 1997, the behavior is different before that year, at least insofar as short-term variations are concerned, and this is discussed further below. The reduction in stratospheric water vapor remains relatively steady from 2001 through the end of 2007 [with a strong quasi-biennial oscillation (QBO) signal in water also present (26)]. Although there is some evidence for a slight increase from mid-

[1]National Oceanic and Atmospheric Administration (NOAA) Earth System Research Laboratory, Chemical Sciences Division, Boulder, CO, USA. [2]Cooperative Institute for Research in Environmental Sciences, University of Colorado, Boulder, CO, USA. [3]Climate and Environmental Physics, Physics Institute, University of Bern, Sidlerstrasse 5, 3012 Bern, Switzerland.
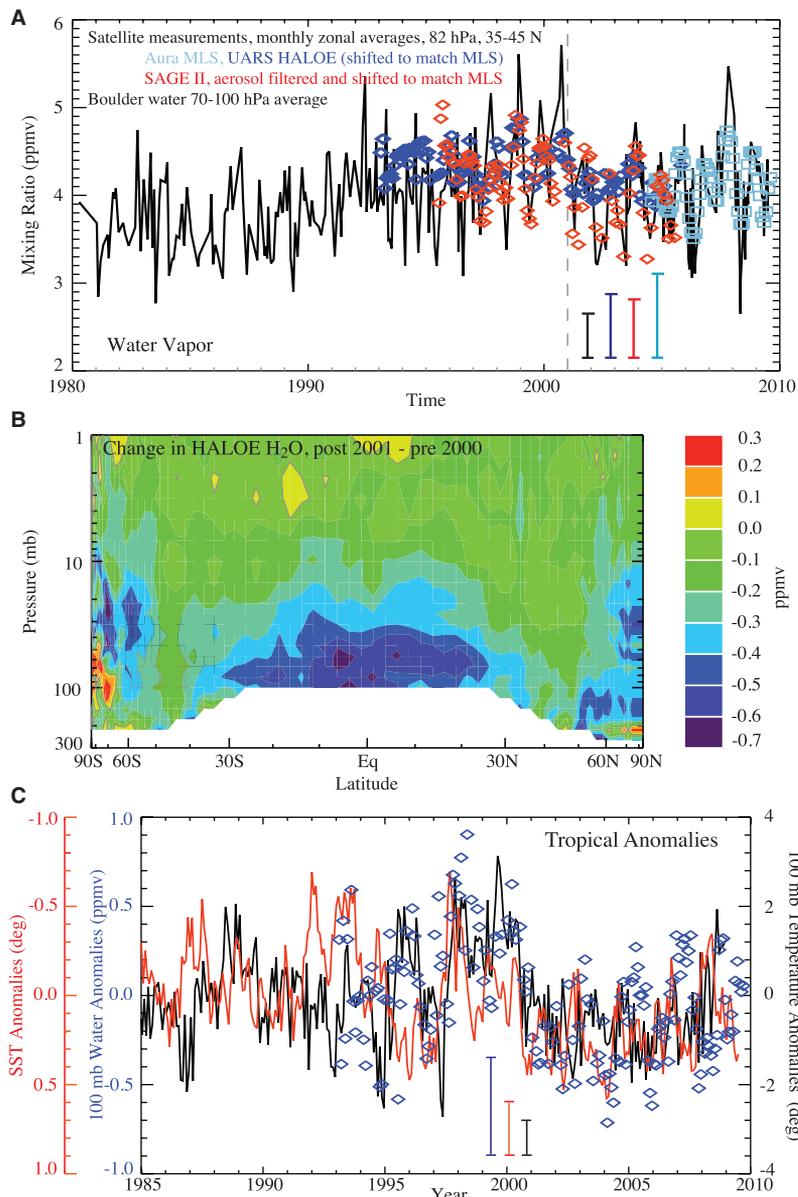
Fig. 1. Observed changes in stratospheric water vapor. (**A**) Balloon measurements of water vapor, taken near Boulder, Colorado (40°N, 105.25°W) along with zonally averaged satellite measurements in the 35° to 45° latitude range at 82 hPa from the Aura MLS (turquoise squares), UARS HALOE (blue diamonds), and SAGE II instruments (red diamonds). The SAGE II and HALOE data have been adjusted to match MLS during the overlap period from mid-2004 to the end of 2005. Representative uncertainties are given by the colored bars; for the satellite data sets, these show the precision as indicated by the monthly standard deviations, while for the balloon data set this is the estimated uncertainty provided in the Boulder data files. (**B**) The altitude/latitude distribution of the drop in HALOE water vapor mixing ratio (in ppmv) in the stratosphere that occurred after 2000. The plot shows the difference between the annual average from June 2001 to May 2005 and the average from January 1996 through December 1999. To extend HALOE data toward the poles, we averaged observations on equivalent latitudes [a coordinate based on potential vorticity that has been used in a variety of satellite studies outside of the subtropics, as in (*36*)], and we then filled any gaps to the pole with the data from the highest equivalent latitude available. (**C**) 10°N to 10°S monthly average anomalies of temperatures and water vapor relative to the period from 1993 to 2006. 100-hPa monthly-averaged temperature anomalies are taken from the Japanese Reanalysis [(*37*), black line], SST anomalies from the Optimal Interpolation Version 2 data obtained from the NOAA Earth System Research Laboratory physical sciences division Web site (www.esrl.noaa.gov/psd) (red line), and 100-hPa water vapor anomalies from the combined UARS HALOE and Aura MLS time series (blue diamonds). Temperatures and SSTs are for longitudinal regions in the Pacific; 139° to 171° for the SSTs, and 171° to 200° for the 100-hPa temperatures, whereas zonal averages are shown for water vapor. Representative uncertainties are given by the colored bars as in (**A**) above and show the average monthly standard deviations.

2007 to mid-2008, the 5-year running mean of the monthly averaged satellite water anomaly in Fig. 1C is nearly flat from 2001 to late 2009 (within ±0.05 ppmv) and is assumed to be constant here.

Radiative effects of stratospheric water vapor changes. Stratospheric water vapor changes affect the fluxes of longwave (infrared) and (to a lesser extent) shortwave (solar) radiation, and can thereby influence the temperature in the stratosphere and troposphere. Radiative transfer calculations were carried out with a high–spectral resolution model (*27*). This accurate line-by-line radiative transfer model integrates over spectral lines to compute the changes in the radiative fluxes at the tropopause when the stratospheric water vapor changes are imposed (the instantaneous radiative forcing). Stratospheric temperatures are then adjusted to the perturbation, using the fixed-dynamical-heating assumption to give the adjusted radiative forcing. The calculation uses an atmosphere derived from the International Satellite Cloud Climatology Project (ISCCP) climatology for temperatures, tropospheric water, and cloud amounts and fractions (*28*). Clouds have only a small effect on the computed radiative forcing, because the water vapor changes considered are in the stratosphere.

The effects of water vapor changes were probed with two sets of radiative transfer calculations. In the first of these, the satellite-based global stratospheric water vapor distributions as discussed above were seasonally averaged above the tropopause for 1996–2000 and 2001.5–2005.5, respectively, to examine the climate impact of the water vapor decrease after 2000. The adjusted radiative forcing of climate from this change was found to be –0.098 W m^{-2}. For comparison, the radiative forcing increase due to the growth of carbon dioxide from 1996 to 2005 was about +0.26 W m^{-2}. In a second case, it was assumed that water vapor had increased uniformly by 1 ppmv at all latitudes and altitudes above the tropopause between 1980 and the 1996–2000 period. A total globally averaged radiative forcing including a stratospheric adjustment of +0.24 W m^{-2} was obtained for this assumed 1-ppmv increase, which is close to the value of +0.29 W m^{-2} reported, for example, in (*3*). This can be compared to the radiative forcing increase due to the growth of carbon dioxide of about +0.36 W m^{-2} from 1980 to 1996. It is clear that carbon dioxide has been increasing for more than a century, whereas the water vapor changes are far shorter in duration, and both the magnitude and time scale of radiative forcing perturbations are important to the resulting surface climate response. The comparison of these radiative forcings nonetheless suggests that the decadal changes in stratospheric water vapor have the potential to affect recent climate, and this is further examined in the next section.

It is informative to investigate the effect of stratospheric water vapor changes at different altitudes on surface climate change by computing

the kernel function for vertical changes (i.e., the radiative forcing per layer). In Fig. 2A we show the kernel function computed using 1-ppmv perturbations of water vapor imposed in 1-km-thick layers. Figure 2A shows that the influence of changes in stratospheric water vapor on shortwave radiation is much smaller than the influence on longwave radiation. Stratospheric adjustment has a large effect on the net radiative forcing in the lowermost stratosphere, where it reduces the impact of local changes there, although they still dominate the profile. Kernel calculations are presented here only for the purpose of illustration, because the full global distributions are used in the detailed radiative calculations discussed above. The kernels should only be considered approximate when convolved with realistic profile changes (comparisons suggest possible errors of between 10 and 25%).

Figure 2A shows that the profile of the kernel function is strongly peaked around the tropopause. The response of surface climate to uniform stratospheric water vapor perturbations would be dominated by this narrow region, at a vertical scale too fine to be captured in many global climate models. Further, the balloon and satellite water vapor records (Figs. 2B and 1) show that the largest observed changes in stratospheric water vapor occurred near the tropopause, so that the shape of the observed stratospheric water perturbation further increases the dominance of the tropopause region in recent radiative forcing. Because of a lack of global data, we have considered only the stratospheric changes, but if the drop in water vapor after 2000 were to extend downward by 1 km, Fig. 2 shows that this would significantly increase its effect on surface climate.

Changes in stratospheric water vapor linked to cold point changes in the tropics are expected to dominate the water vapor variations in the lowermost stratosphere and are transported laterally to mid-latitudes on time scales of months to at most a few years. Thus, the gradual and persistent water vapor increase observed at Boulder from 1980 to 2000 as shown in Fig. 1A should reflect similar changes occurring elsewhere in the altitude range of greatest importance for radiative forcing. Nevertheless, the data before the mid-1990s are limited in space and/or time, and the stratospheric water vapor trends before 2000 should therefore be considered uncertain, whereas the decrease after 2000 is much better characterized by multiple records.

Methane oxidation increases stratospheric water vapor, but its contributions are small near the tropopause (29), the region of greatest impact for radiative forcing as shown in Fig. 2. This explains why studies in which methane oxidation is the only adopted source of increasing stratospheric water provide considerably smaller radiative forcings than those shown here. Estimates of the forcing due to methane oxidation have varied widely among different studies (30), perhaps because of different shapes of the water profile in the region of greatest sensitivity. Such differences are a source of potential confusion about the influence of stratospheric water vapor changes on surface climate, and they underscore the need to consider the direct input of water vapor at the cold point.

Global temperature response. We used the Bern 2.5CC intermediate complexity model (31) to estimate the effect of the decrease in stratospheric water vapor after 2000 on recent global average decadal temperature trends. The model

has been extensively compared to other Earth system models of intermediate complexity as well as to atmosphere-ocean general circulation models [AOGCMs (31)]. A radiative forcing time series of well-mixed greenhouse gases and tropospheric aerosols from 1760 to 2008 was used to provide a baseline model scenario to which cases including stratospheric water vapor changes are compared (additional forcings such as tropospheric ozone were not considered). The resulting total radiative forcing and calculated temperature changes relative to 1980 are shown in Fig. 3, together with observed annual average surface temperature anomalies from three different global temperature data sets for individual years (32), and for the 5-year running mean. Absolute values of the calculated temperature changes are dependent on the model climate sensitivity and transient climate response and are hence somewhat arbitrary. The focus here is therefore not on the detailed match to observed absolute warming but rather on the changes in radiative forcing and their likely implications for relative changes in the decadal rates of warming from 1980 to 2009.

Figure 3 shows the added forcing and estimated warming corresponding to an adopted linear increase of stratospheric water vapor forcing ranging from 0 to +0.24 W m^{-2} from 1980 to 2000 based on the analysis in the previous section. This range brackets the large uncertainty in water vapor trends before 2000. The figure also shows the effect of the observed post-2000 decrease, for which there is much higher confidence as discussed above. Figure 3 shows that the reduced forcing associated with the drop in stratospheric water vapor after 2000 decreased the rate of warming as compared to what would have been expected for well-mixed greenhouse gases alone by about 25% (from about 0.14°C per decade to 0.10°C per decade for this particular model or about a –0.04°C per decade change). Figure 3 also shows that an increase in global stratospheric water vapor at the upper end of the range suggested by the balloon measurements should be expected to have steepened the rate of global warming from 1990 to 2000 by about 30% as compared to a case neglecting stratospheric water changes.

Figure 3 thus shows that the decline in stratospheric water vapor after 2000 should be expected to have significantly contributed to the flattening of the global warming trend in the past decade, and stratospheric water increases may also have acted to steepen the observed warming trend in the 1990s. The transient climate response (TCR) of the model used in Fig. 3 is slightly less than the mean of models assessed by the Intergovernmental Panel on Climate Change (IPCC) (1); the "very likely" range of TCR across climate models suggests that the effects of the stratospheric water vapor changes on the warming trends considered here could be greater by about 80% or smaller by about 40%. Our analysis focuses only on estimating the contributions of stratospheric water vapor changes to recent decadal rates of warming;
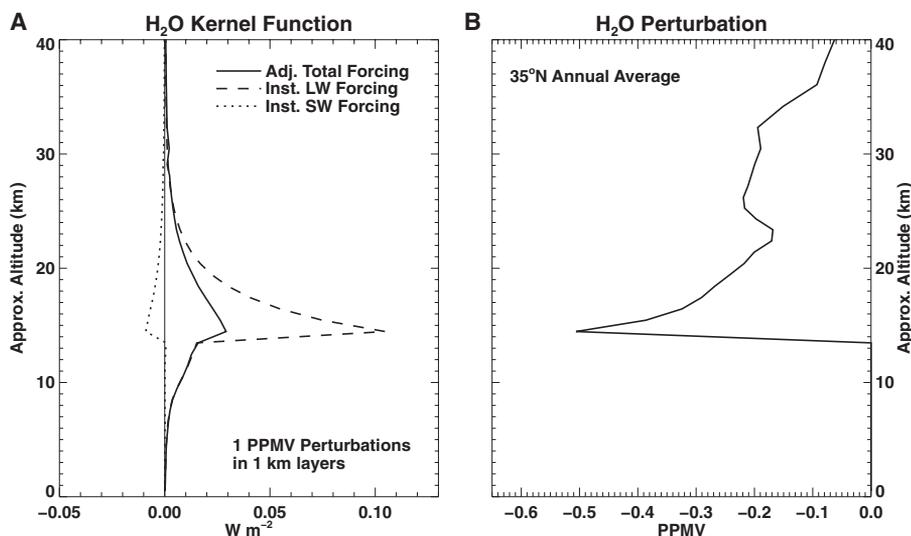
Fig. 2. Effect of stratospheric water vapor changes on radiative forcing of surface climate based on detailed line-by-line calculations. (**A**) Instantaneous longwave (LW) and instantaneous shortwave (SW) radiative forcing, along with the adjusted net total forcing versus altitude at 35°N obtained for a uniform change of 1 ppmv in 1-km layers using a line-by-line radiative transfer model; the largest sensitivity occurs close to the tropopause. (**B**) The observed post-2000 water vapor decrease at 35°N (from Fig. 1B), showing that the largest changes occurred in the most sensitive region.

A Radiative Forcing Change From 1980

B Temperature Change From 1980

C Impact of Stratospheric H₂O Changes on Decadal Temperature Trends
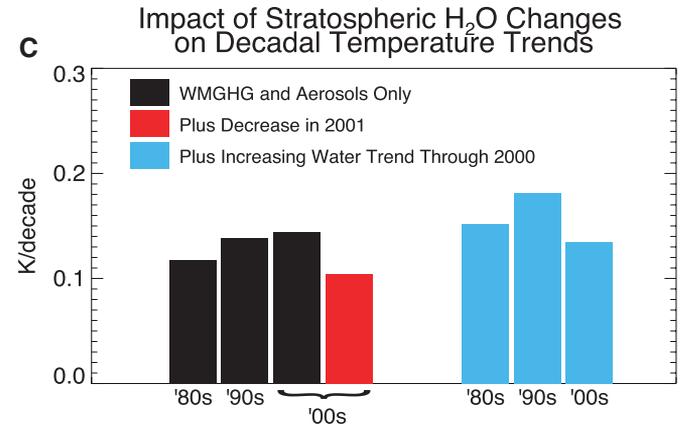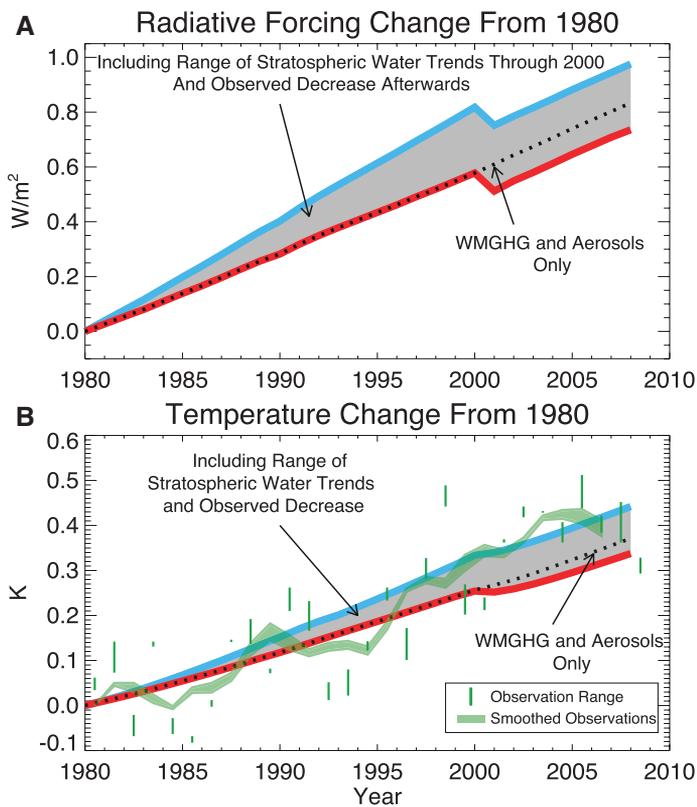
Fig. 3. Impact of changes in stratospheric water vapor on surface climate. (**A**) Time series of the changes in radiative forcing since 1980 due to well-mixed greenhouse gases (WMGHG), aerosols, and stratospheric water vapor. The forcings of CO_2, CH_4, and N_2O are obtained from historical mixing ratios (38). The forcing of the Montreal Protocol gases is calculated from their radiative efficiencies and observed mixing ratio time series (39). The time dependence of the tropospheric aerosol forcing is taken from Goddard Institute for Space Studies (GISS) model input (http://data.giss.nasa.gov/modelforce/RadF.txt), but scaled so that total aerosol radiative forcing from 1985 to 2004 is −1.1 W m^{-2}, following (40). The shaded region shows the stratospheric water contribution calculated from an assumed range of decadal trends from 1980 to 2000 of 0 (red line) to 0.5 ppmv per decade (blue line) along with the observed decline prescribed after 2000. (**B**) Measured and modeled temperature changes relative to 1980. Three different observed global temperature records were used [from the National Climate Data Center (NCDC), Climatic Research Unit (CRU), and GISS records], with the green markers indicating the range across the three data sets in each year. The green shaded line shows the range of the 5-year running mean of the three data sets. (**C**) Decadal warming rates arising from (i) the WMGHG and aerosols alone (black), as well as (ii) that obtained including the stratospheric water decline after 2000 (red) and (iii) including both the stratospheric water vapor decline after 2000 and the increase in the 1980s and 1990s (cyan). Smooth lines show the warmings calculated by the Bern intermediate complexity climate model, which does not simulate internal variability from one year to another. Volcanoes have not been included in the radiative forcing. The climate sensitivity of the model used is 3°C for a doubling of atmospheric CO_2, and the transient climate response is 1.7°C, slightly less than the mean of the range of models assessed by the IPCC (1). The colors of the bars in (C) correspond to the respective lines shown in (A) and (B).

additional contributions such as from solar variations (33), aerosols, natural variability, or other processes are not ruled out by this study.

Recent observations have suggested a correlation of the post-2000 stratospheric water vapor decrease with SST changes near the tropical warm pool region and associated cooling of the cold point that governs water vapor input to the stratosphere in the tropics (Fig. 1C). However, the relation between SSTs in the warm pool region and stratospheric water vapor changes character (from negative to positive short-term correlations) from 1980 to 2009, suggesting that other processes may also be important or that the correlation may be a transient feature linked to the specific pattern of SSTs at a given time rather than to the average warming of SSTs around the globe. It is therefore not clear whether the stratospheric water vapor changes represent a feedback to global average climate change or a source of decadal variability. Current global climate models suggest that the stratospheric water vapor feedback to global warming due to carbon dioxide increases is weak (1, 34), but these models do not fully resolve the tropopause or the cold point, nor do they completely represent the QBO, deep convective

transport and its linkages to SSTs, or the impact of aerosol heating on water input to the stratosphere (35). This work highlights the importance of using observations to evaluate the effect of stratospheric water vapor on decadal rates of warming, and it also illuminates the need for further observations and a closer examination of the representation of stratospheric water vapor changes in climate models aimed at interpreting decadal changes and for future projections.

References and Notes
1. IPCC, *Climate Change 2007: The Physical Science Basis*, Contribution of Working Group I to the Fourth Assessment Report of the Intergovernmental Panel on Climate Change, S. Solomon et al., Eds. (Cambridge Univ. Press, Cambridge, 2007).
2. D. R. Easterling, F. M. Wehner, *Geophys. Res. Lett.* **36**, L08706 (2009).
3. P. M. de S. Forster, K. P. Shine, *Geophys. Res. Lett.* **26**, 3309 (1999).
4. C. A. Smith, J. D. Haigh, R. Toumi, *Geophys. Res. Lett.* **28**, 179 (2001).
5. D. T. Shindell, *Geophys. Res. Lett.* **28**, 1551 (2001).
6. K. E. Trenberth, J. Fasullo, L. Smith, *Clim. Dyn.* **24**, 741 (2005).
7. A. E. Dessler, Z. Zhang, P. Yang, *Geophys. Res. Lett.* **35**, L20704 (2008).
8. P. W. Mote et al., *J. Geophys. Res.* **101**, (D2), 3989 (1996).
9. E. C. Cordero, P. M. Forster, *Atmos. Chem. Phys.* **6**, 5369 (2006).
10. A. Gettleman et al., *Atmos. Chem. Phys.* **9**, 1621 (2009).
11. R. R. Garcia, D. R. Marsh, D. E. Kinnison, B. A. Boville, F. Sassi, *J. Geophys. Res.* **112**, (D2), D09301 (2007).
12. V. Oinas, A. A. Lacis, D. Rind, D. T. Shindell, J. E. Hansen, *Geophys. Res. Lett.* **28**, 2791 (2001).
13. D. Kley et al., *SPARC Assessment of Upper Tropospheric and Stratospheric Water Vapour* [WCRP-No. 113, WMO/TD No. 1043S, SPARC Report No. 2, Stratospheric Processes and Their Role in Climate (SPARC) project, World Meteorological Organization, Paris, 2000].
14. S. J. Oltmans, H. Vomel, D. J. Hofmann, K. H. Rosenlof, D. Kley, *Geophys. Res. Lett.* **27**, 3453 (2000).
15. W. J. Randel, F. Wu, H. Vomel, G. E. Nedoluha, P. M. D. Forster, *J. Geophys. Res.* **111**, (D12), D12312 (2006).
16. J. E. Harries et al., *J. Geophys. Res.* **101**, (D6), 10205 (1996).
17. M. Scherer, H. Vomel, S. Fueglistaler, S. J. Oltmans, J. Staehelin, *Atmos. Chem. Phys.* **8**, 1391 (2008).
18. D. Rind et al., *J. Geophys. Res.* **98**, (D3), 4835 (1993).
19. A. Lambert et al., *J. Geophys. Res.* **112**, (D24), D24S36 (2007).
20. K. H. Rosenlof et al., *Geophys. Res. Lett.* **28**, 1195 (2001).
21. A. W. Brewer, *Q. J. R. Meteorol. Soc.* **75**, 351 (1949).
22. J. R. Holton et al., *Rev. Geophys.* **33**, 403 (1995).
23. S. C. Sherwood, A. E. Dessler, *J. Atmos. Sci.* **58**, 765 (2001).
24. S. Fueglistaler et al., *Rev. Geophys.* **47**, RG1004 (2009).

25. K. Rosenlof, G. C. Reid, *J. Geophys. Res.* **113**, (D6), D06107 (2008).
26. M. A. Geller, X. L. Zhou, M. H. Zhang, *J. Atmos. Sci.* **59**, 1076 (2002).
27. R. W. Portmann *et al.*, *J. Geophys. Res.* **102**, (D8), 9409 (1997).
28. W. B. Rossow, R. A. Schiffer, *Bull. Am. Meteorol. Soc.* **80**, 2261 (1999).
29. S. Rohs *et al.*, *J. Geophys. Res.* **111**, (D14), D14315 (2006).
30. P. Forster *et al.*, in (*1*), pp. 129–234.
31. G.-K. Plattner *et al.*, *J. Clim.* **21**, 2721 (2008).
32. K. Trenberth *et al.*, in (*1*), pp. 235–336.
33. J. L. Lean, D. H. Rind, *Geophys. Res. Lett.* **36**, L15708 (2009).
34. N. Stuber, M. Ponater, R. Sausen, *Clim. Dyn.* **24**, 497 (2005).
35. S. Sherwood, *Science* **295**, 1272 (2002).
36. G. Manney *et al.*, *J. Geophys. Res.* **112**, D24S50 (2007).
37. K. Onogi *et al.*, *J. Meteorol. Soc. Jpn.* **85**, 369 (2007).
38. J. M. Gregory, P. M. Forster, *J. Geophys. Res.* **113**, D23105 (2008).
39. World Meteorological Organization, *Scientific Assessment of Ozone Depletion: 2006* (Global Ozone Research and Monitoring Project-Report No. 50, Geneva, Switzerland, 2007).
40. D. M. Murphy *et al.*, *J. Geophys. Res.* **114**, D17107 (2009).
41. This work was supported by the Atmospheric Composition and Climate Program of the National Oceanic and Atmospheric Administration Climate Program. We appreciate helpful comments on a draft manuscript by K. Shine, M. Geller, A. Gettelman, and A. Dessler.

Sestrin as a Feedback Inhibitor of TOR That Prevents Age-Related Pathologies

Jun Hee Lee,[1] Andrei V. Budanov,[1] Eek Joong Park,[1] Ryan Birse,[2] Teddy E. Kim,[3] Guy A. Perkins,[4] Karen Ocorr,[2] Mark H. Ellisman,[4] Rolf Bodmer,[2] Ethan Bier,[3]* Michael Karin[1]*

Sestrins are conserved proteins that accumulate in cells exposed to stress, potentiate adenosine monophosphate–activated protein kinase (AMPK), and inhibit activation of target of rapamycin (TOR). We show that the abundance of *Drosophila* sestrin (dSesn) is increased upon chronic TOR activation through accumulation of reactive oxygen species that cause activation of c-Jun amino-terminal kinase and transcription factor Forkhead box O (FoxO). Loss of dSesn resulted in age-associated pathologies including triglyceride accumulation, mitochondrial dysfunction, muscle degeneration, and cardiac malfunction, which were prevented by pharmacological activation of AMPK or inhibition of TOR. Hence, dSesn appears to be a negative feedback regulator of TOR that integrates metabolic and stress inputs and prevents pathologies caused by chronic TOR activation that may result from diminished autophagic clearance of damaged mitochondria, protein aggregates, or lipids.

Target of rapamycin (TOR) is a key protein kinase that regulates cell growth and metabolism to maintain cellular and organismal homeostasis (*1–3*). Insulin and insulin-like growth factors are major TOR activators that operate through phosphoinositide 3-kinase (PI3K) and the protein kinase AKT (*2*). Conversely, adenosine monophosphate–activated protein kinase (AMPK), which is activated upon energy depletion, caloric restriction (CR), or genotoxic damage, is a stress-responsive inhibitor of TOR activation (*2, 4*). TOR stimulates cell growth and anabolism by increasing protein and lipid synthesis through p70 S6 kinase (S6K), eukaryotic translation initiation factor 4E-binding protein (4E-BP), and sterol response element binding protein (SREBP) (*1–3, 5*) and by decreasing autophagic catabolism through

phosphorylation-mediated inhibition of ATG1 protein kinase (*1, 6*). Persistent TOR activation is associated with diverse pathologies such as cancer, diminished cardiac performance, and obesity-associated metabolic diseases (*1*). Conversely, inhibition of TOR prolongs life span and increases quality of life by reducing the incidence of age-related pathologies (*1–3, 7*). The antiaging effects of CR could be due to inhibition of TOR (*8*).

Sestrins (Sesns) are highly conserved proteins that accumulate in cells exposed to stress, lack obvious domain signatures, and have poorly defined physiological functions (*9, 10*). Mammals express three Sesns, whereas *Drosophila melanogaster* and *Caenorhabditis elegans* have single orthologs (fig. S1, A and B). In vitro, Sesns exhibit oxidoreductase activity and may function as antioxidants (*11*). Independently of their redox activity, Sesns lead to AMPK-dependent inhibition of TOR signaling and link genotoxic stress to TOR regulation (*12*). However, Sesns are also widely expressed in the absence of exogenous stress, and in *Drosophila*, expression of *Drosophila* sestrin (dSesn) is increased upon maturation and aging (fig. S1C) (*10*). Given the redundancy between mammalian Sesns, we chose to test the importance of Sesns as regulators of TOR function in *Drosophila*. We

generated both gain- and loss-of-function *dSesn* mutants (figs. S2 to S4). Analysis of these mutants revealed that dSesn is an important negative feedback regulator of TOR whose loss results in various TOR-dependent, age-related pathologies (*13*).

Prolonged TOR signaling induces dSesn. Persistent TOR activation in wing discs by a constitutively active form of the insulin receptor (InR[CA]) resulted in prominent dSesn protein accumulation, which is not seen in a *dSesn*-null larvae (Fig. 1, A to C). InR[CA] also induced accumulation of *dSesn* RNA (Fig. 1, D to F), indicating that dSesn accumulation is due to increased transcription or mRNA stabilization. As dSesn accumulation was restricted to cells in which TOR was activated, the response is likely to be cell autonomous. dSesn was also induced when TOR was chronically activated by over-expression of the small guanine triphosphatase Rheb (Fig. 1G), clonal loss of phosphatase and tensin homolog (PTEN), or tuberous sclerosis complex 1 (TSC1) (Fig. 1, H and I). Dominant-negative PI3K (PI3K[DN]) or TOR (TOR[DN]) inhibited dSesn accumulation caused by over-expression of InR[CA], but inactive ribosomal S6 protein kinase (S6K, S6K[DN]) and hyperactive 4E-BP (4E-BP[CA]), two downstream TOR effectors, did not (fig. S5). Furthermore, dorsal-specific expression of activated S6K[CA] or loss of 4E-BP activity failed to induce dSesn expression (Fig. 1, J and K), indicating that TOR regulates expression of dSesn through different effector(s).

TOR signaling generates ROS to induce dSesn. In mammals, transcription of *Sesn* genes is increased in cells exposed to oxidative stress (*9, 11*), and we observed reactive oxygen species (ROS) accumulation, detected by oxidation of dihydroethidium (DHE), in the same region of the imaginal discs in which InR[CA] or Rheb were expressed (Fig. 2, A and B). InR[CA]-induced accumulation of ROS was blocked by coexpression of either PI3K[DN] or TOR[DN], but not S6K[DN] or 4E-BP[CA] (Fig. 2B), revealing TOR's role in ROS accumulation. Wing-disc clones in which TOR was activated by loss of TSC1 also exhibited ROS accumulation (Fig. 2C), confirming that TOR-dependent ROS accumulation is cell-autonomous. Expression of the ROS scavengers catalase or peroxiredoxin (*14*) inhibited InR[CA]-induced accumulation of dSesn

[1]Laboratory of Gene Regulation and Signal Transduction, Departments of Pharmacology and Pathology, School of Medicine, University of California San Diego (UCSD), La Jolla, CA 92093–0723, USA. [2]Development and Aging Program, Neuroscience, Aging and Stem Cell Research Center, Sanford-Burnham Medical Research Institute, La Jolla, CA 92037, USA. [3]Section of Cell and Developmental Biology, UCSD, La Jolla, CA 92093–0349, USA. [4]National Center for Microscopy and Imaging Research and Department of Neurosciences, UCSD, La Jolla, CA 92093–0608, USA.

*To whom correspondence should be addressed. E-mail: ebier@ucsd.edu (E.B.); karinoffice@ucsd.edu (M.K.)